IAC-19-D2.4.2

European Next Reusable Ariane (ENTRAIN): A Multidisciplinary Study on a VTVL and a VTHL Booster Stage

Sven Stappert[a]*, Jascha Wilken[a], Leonid Bussler[a], Martin Sippel[a], Sebastian Karl[b], Josef Klevanski[c], Christian Hantz[c], Lâle Evrim Briese[d], Klaus Schnepper[d]

[a] *German Aerospace Center (DLR), Institute of Space Systems, Robert-Hooke-Straße 7. 28359 Bremen, Germany*
[b] *German Aerospace Center (DLR), Institute of Aerodynamics and Flow Technology, Bunsenstrasse 10, 37073 Göttingen, Germany*
[c] *German Aerospace Center (DLR), Institute of Aerodynamics and Flow Technology, Linder Höhe, 51147 Köln, Germany*
e German Aerospace Center (DLR), Institute of System Dynamics and Control, 82234,Oberpfaffenhofen, Germany
* Corresponding Author

Abstract

The recent success of the emerging private space companies SpaceX and Blue Origin in landing, recovering and relaunching reusable first stages have demonstrated the possibility of building reliable and low-cost reusable first stages. Thus, the importance for assessing whether such a reusable launch vehicle (RLV) could be designed and built in Europe has increased. Due to this renewed interest in RLVs, the German Aerospace Center (DLR) has initiated a study on reusable first stages named ENTRAIN (**E**uropean **N**ex**t** **R**eusable **Ari**a**n**e). Within this study two return methods, respectively vertical take-off, vertical landing (VTVL) and vertical take-off, horizontal landing (VTHL) with winged stages, are investigated. The goal is to assess the impact of the return method on the launcher and to conduct a preliminary design of a possible future European RLV.

In the first part of the study, which ended in 2018, a broad range of possible launcher designs considering different propellant combinations, engine cycles and staging velocities were investigated and compared. By the end of this part, the most promising VTVL stage such as the most promising VTHL stage were selected to be investigated in more detail. Those two concepts were subjected to a preliminary system design and performance estimation, coupled with an aerodynamic and aerothermodynamic investigation of the re-entry loads and their impact on the structure. Furthermore, analyses of the dynamic behavior of descending RLV stages are considered. With the know-how gained within this study, the design of both launchers shall be enhanced to a level that brings it closer to a viable future reusable European launcher.

Keywords: RLV, VTVL, VTHL, ENTRAIN, Reusability, Re-entry

Acronyms/Abbreviations

AEDB	Aerodynamic Database
AETDB	Aerothermodynamic Database
AoA	Angle of Attack
ASDS	Autonomous Spaceport Droneship
BEO	Beyond Earth Orbit
DRL	Downrange Landing
ELV	Expendable Launch Vehicle
ENTRAIN	European Reusable Next Ariane
GTO	Geostationary Transfer Orbit
Isp	Specific Impulse
L/D	Lift-to-Drag Ratio
LCH4	Liquid Methane
LH2	Liquid Hydrogen
LOX	Liquid Oxygen
MEO	Medium Earth Orbit
RCS	Reaction Control System
RLV	Reusable Launch Vehicle
SI	Structural Index
SSO	Sun-synchronous Orbit
TPS	Thermal Protection System
VTHL	Vertical Take-off, Horizontal Landing
VTVL	Vertical Take-Off, Vertical Landing

1. Introduction

While reusability in space transportation can have a strong impact on the costs and thus competitiveness of space launchers, the historic Space Shuttle has also shown that this impact does not necessarily have to be positive if the refurbishment costs cannot be kept low. Nonetheless, the recent success of SpaceX (with Falcon 9 and Falcon Heavy) and Blue Origin (New Shephard) in landing, recovering and reusing their respective booster stages by means of retropropulsion have shown the possibility of developing, producing and operating reusable launchers at low launch service costs. This has raised the interest in introducing reusability to European launchers as a way to lower the launch costs and stay competitive on the evolving launch market. Reusability

for launch systems can be achieved through a broad range of different technologies and approaches. Understanding and evaluating the impact of the different possible return and reuse methods on a technological, operational and economic level is of essential importance for choosing a technology that is adaptable to a European launch system.

Fig. 1: SpaceX Falcon Heavy side booster using the VTVL method (left; photo by SpaceX; CC0 1.0) and the LFBB representing the VTHL method (right)

In order to assess those demands of reusable launch vehicles, the DLR project X-TRAS was initiated. In the first phase of the study, which ended in 2018, a broad range of preliminary designed RLV concepts were compared to each other with respect to different parameters such as performance, mass, re-entry trajectory and loads. In this phase, several design parameters such as propellant combination, upper stage Δv, engine cycle and return modes were subject to variation to identify advantages and disadvantages and optimal design points of each configuration [1], [2]. At the end, one promising VTVL and one promising VTHL concept were selected to be investigated in much more detail. The selected VTVL concept is propelled by LOX/LCH4 in the reusable first stage and LOX/LH2 in the second stage and is designed for downrange landings on a barge. The VTHL launcher is propelled by LOX/LH2 and is supposed to be captured in-air by a towing aircraft after re-entry (see Fig. 2) [3].

The goal of this second phase of the ENTRAIN study, dubbed ENTRAIN2, is the detailed investigation by using sophisticated methods and tools to achieve an in-depth understanding of the design challenges of a RLV. Hence, a detailed aerodynamic and aerothermodynamic investigation of the two launcher concepts was performed to determine the re-entry environment and loads and aerodynamic demands and their impact on the trajectory. Furthermore, a preliminary analysis of flight dynamics and control issues is performed. The work performed within ENTRAIN2 shall allow a detailed analysis of promising RLV concepts that might be adaptable to a future European launch system.

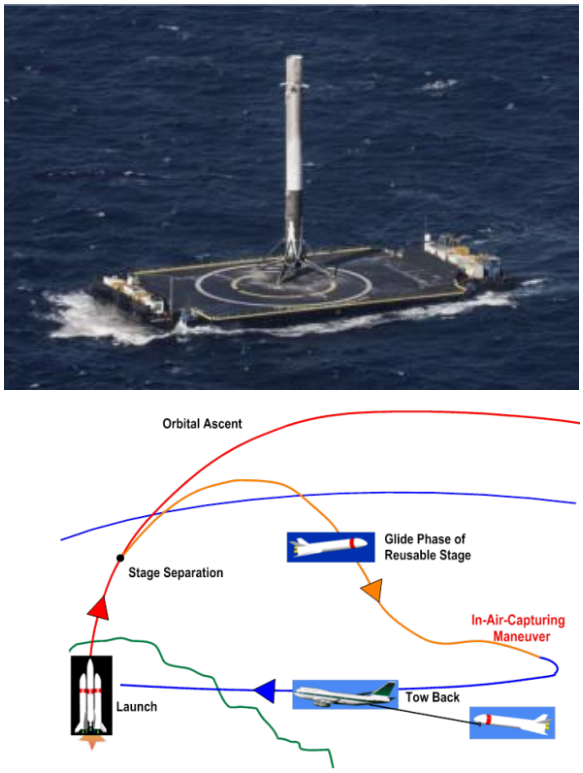

Fig. 2: SpaceX Falcon 9 landed stage on a ASDS (left, Photo by SpaceX; CC0 1.0) and sketch of an In-Air-Capturing mission (right)

2. Study Methodology and Mission Requirements

As mentioned earlier, the first part of the ENTRAIN ended in 2018. Results of this part are presented in detail in [1], [2], [4]. The insights gained by this first part were used to select two promising concepts: one VTVL launcher and one VTHL launcher.

The VTVL launcher selected by the end of this first part consists of an RLV first stage using LOX/LCH4 as propellants and an expendable second stage using LOX/LH2 as propellants. The major advantages of that

design are a relatively low dry mass and the compatibility with methane engines, thus allowing the future methane engine Prometheus to be possibly used as first stage engines. However, in this paper the generic methane gas generator engines from the first ENTRAIN study part were used [1]. A major disadvantage of the design as hybrid launcher is the resulting necessity of developing two different engines. The VTVL RLV is designed for a payload mass of 5.5 t into GTO with a downrange landing on a barge offshore of Kourou, similar to what SpaceX is doing with its Falcon 9. Additionaly, the VTVL launcher is also capable of doing RTLS for low-energy orbits such as LEO or SSO (see section 3 for details).

As VTHL reference concept a LOX/LH2 fueled first and second stage using gas generator engines was selected. The stage shall perform In-Air-Capturing, thus neglecting the need of turbine engines and additional propellants to perform an autonomous flyback to the landing site. The advantages of this concept are a low dry mass and the development and use of one engine with different expansion ratios for both stages. Furthermore, the performance losses of IAC were shown to be the lowest of all considered RLV configurations [1]. The VTHL concept was designed to deliver a payload of 7.5 t into the reference GTO.

While the VTVL configuration has a lower payload capacity in DRL-mode, as an expendable version its performance in GTO is still large enough to lift the heaviest missions of the mission scenario of 7.5 tons into GTO. This effectively limits the number of reuses since every heavy-lift launch has to be performed as expendable vehicle. More detail is given in section 3.

For both concepts, similar target orbits and mission scenarios were assumed which are explained in detail in section 0 and 2.1. Those assumptions were used to determine payload capabilities, market serving capabilities and trajectories (section 3). Section 4 focuses on the aerodynamic and aerothermodynamic design based on the trajectories obtained and section 5 explains the basic preliminary system dynamics evaluation performed on the ENTRAIN2 launcher concepts.

Target Orbits

In this paper the payload performance of both launchers into different target orbits are considered. As mentioned in the previous section, the reference target orbit is a GTO orbit with launch from Kourou. Additionally, the performances into LEO, MEO and SSO were considered. The target orbital parameters are as follows:

GTO: 250 km × 35786 km, 6° inclination via transfer orbit of 160 km x 330 km

LEO (ISS delivery orbit): 330 km x 330 km x 51.6° via launcher dependent transfer orbit

SSO: 700 km x 700 km x 97.4° via launcher dependent transfer orbit

MEO: 23200 km x 23200 km x 56° (Galileo Satellite Orbit) via transfer orbit of 200 km x 23200 km

Launch from Kourou, French Guyana: 5.24° N / 52.77° W

The GTO orbit described above is reached via a two burn strategy due to the requirement that the argument of perigee has to be 0° or 180° (perigee and apogee on equatorial plane). Hence, the launchers are first accelerated into the transfer orbit of 160 km x 330 km followed by a coasting phase. When reaching the equatorial plane, the second engine is reignited to provide the final Δv necessary to reach the desired GTO (see Fig. 3).

For all other orbits the final parameters are identical. However, the final orbits are reached by different transfer orbits that are dependent on the launcher. The VTVL first stage requires rather steep trajectories with a high flight path angle at MECO when opting for a return

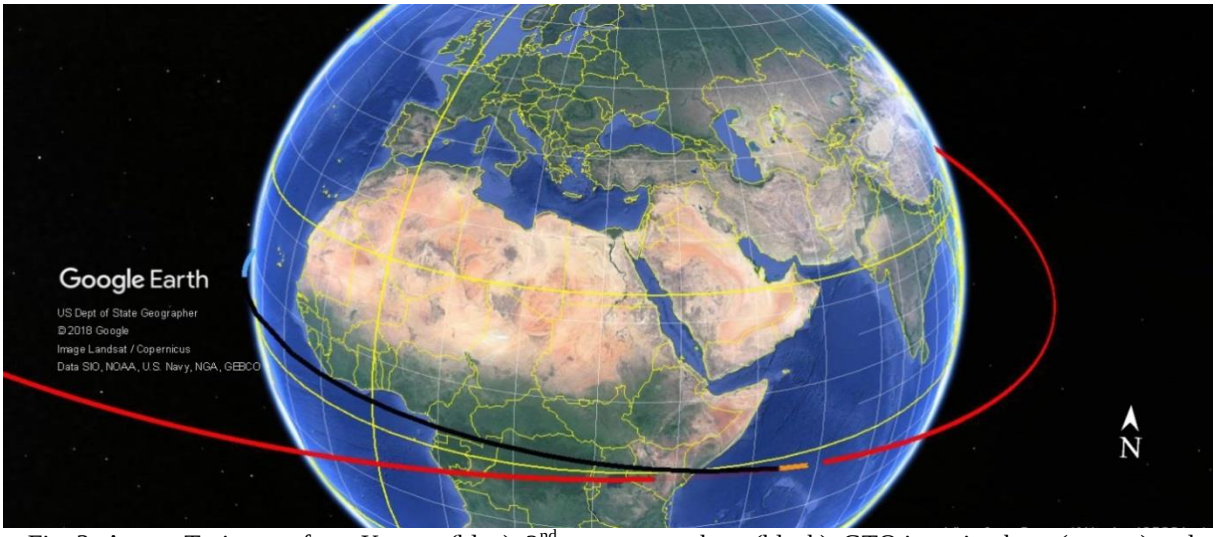

Fig. 3: Ascent Trajectory from Kourou (blue), 2nd stage coast phase (black), GTO insertion burn (orange) and final GTO (red)

to launch site. Contrary, a flat flight path angle is favorable for barge landings since the deceleration of the returning stage via aerodynamic forces is greater in that case (see [1]-[5] for details).

In the case of VTHL transfer orbits, rather flat trajectories are advantageous in general. This can be explained by the fact that the returning first stage can decelerate by aerodynamic means only. In the case of a flat trajectory with a low re-entry path angle the aerodynamic forces are building up less rapidly compared to steep re-entries. This allows for greater control and reduces the maximum heat flux during re-entry.

2.1. *Future Market Scenario*

The evaluation of the designed VTVL and VTHL launcher is conducted taking different market scenarios into account. Thus, the number of required launches per year shall be derived and the launchers market serving capability determined. In the context of the ENTRAIN study, three different market scenarios were defined: a pessimistic scenario, a "most probable" market scenario and an optimistic scenario. In this paper, only the "most probable" market scenario was selected to evaluate the launchers' capabilities. This scenario is composed of the following mission requirements as shown in Table 1.

Table 1: Market Scenario and assumed launches per year for the ENTRAIN2 RLV launchers

Market	Mission & Mass Payload	
Institutional	GTO	1 x 4 t
	MEO (Galileo)	3 x 1 t
	SSO	2.5 x1.5 t + 1 x 4t
	BEO	0.33 x 3 t +0.16 x Performance Max.
Commercial	GTO	3 x 3 t + 3 x 5 t + 3 x 7 t
	SSO	0.5 x 1.5 t
Constellation	LEO	20 t per year

3. System Design & Performance

3.1. Engine Parameters

The engines used in both concepts are scaled version of the generic engines used throughout the study. The assumptions and methods have been presented in detail in [6]. Only the expansion ratio was optimized within the aforementioned preliminary design studies for the relevant case. For the upper stage the expansion ratio was limited by the final size of the nozzle, so that the upper stage engine of the VTHL was limited to an expansion ratio of 120 while the smaller VTVL upper stage engine could have an expansion ratio of 150 while keeping the nozzle at a feasible size.

For the first stage the maximum expansion ratio of the VTVL was limited by the throttling requirement in order to not cause flow separation during the descent, which could damage the nozzle. The final performance parameters of the engines are given in Table 2.

Table 2: Engine Parameters

Launcher	**VTVL**		**VTHL**	
Stage	1st	2nd	1st	2nd
Propellants	LOX/ LCH4	LOX/ LH2	LOX/LH2	
Cycle	Gas generator		Gas generator	
MCC pressure	12 MPa	12 MPa	12 MPa	12 MPa
Expansion ratio	22	150	31	120
Isp, sea level	288 s	-	356 s	-
Thrust, SL	748 kN	-	768 kN	-
Isp, vacuum	322.5 s	444 s	416 s	440 s
Thrust, vacuum	838 kN	635 kN	897 kN	950 kN
Number of Engines in stage	9	1	7	1

3.2. VTVL – System Design and Performance

The VTVL system is designed as TSTO configuration with a reusable VTVL first stage and an expendable stage in tandem configuration. The geometry and layout of the launcher is shown in Fig. 4. The first stage roughly consists of (from bottom to top) 9 LOX/methane engines, a rear skirt which protects the thrust frame and the engines and engine equipment, the LCH4 tank which is separated by a common bulkhead from the LOX tank and an interstage that accommodates the second stage's engine nozzle during ascent. The first stage is further equipped with four planar fins to allow for aerodynamic control in the denser parts of the atmosphere. The fins are folded in ascent configuration but are unfolded following separation from the second stage (see Fig. 5). Furthermore, four landing legs are attached to the rear end of the stage which extend and lock in the final seconds prior to the stage's landing. The design of those legs is based on the landing leg design of the VTVL demonstrator CALLISTO [7].

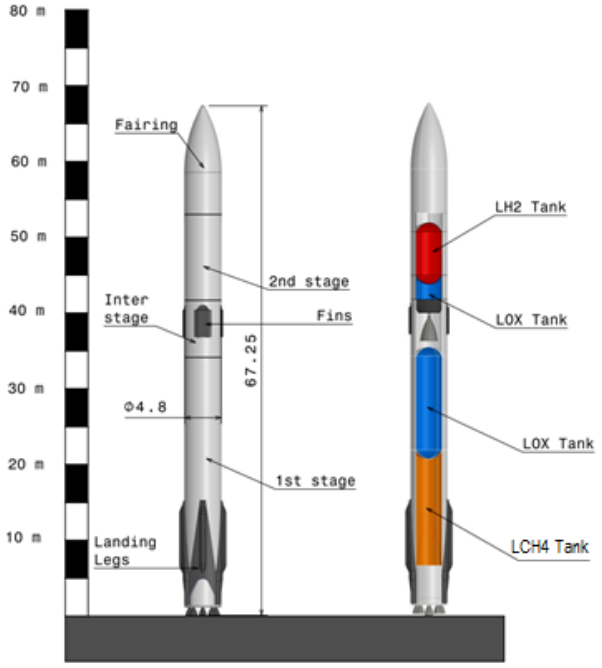

Fig. 4: VTVL Launcher dimensions and internal layout

The second stage is made up of the LOX and LH2 tanks which are also separated by a common bulkhead. A front skirt is attached to the front end of the LH2 tank to accommodate the avionics and flight control hardware and the second stage power supply. The payload adapter is attached to the front skirt and provides structural support of the payload which is covered by an ogive fairing during ascent.

The launcher's mass breakdown is provided in Table 3. The masses were calculated with preliminary sizing and mass estimation tools. The masses of first and second stage tanks such as all skirts and the interstage were calculated using the in-house structural analysis tool *lsap*. This tool calculates the necessary stringer-frame layout and resulting structural mass considering a range of failure cases. The mass of the fairing was calculated by scaling the RLV's fairing area with the fairing area of the Ariane 5. Planar fin and landing leg masses were derived by scaling the respective masses of the Falcon 9 launcher. It is important to note that the Falcon 9 masses were derived using in-house tools and reverse engineering assumptions, thus naturally being subject to uncertainties [8]. A preliminary TPS, consisting of a cork layer of 2 cm thickness covering the whole baseplate, was assumed.

$$SI = \frac{m_{dry}}{m_{propellant}} \quad (1)$$

Fig. 5: VTVL reusable first stage in descent configuration with fins extended

Table 3: Mass Breakdown of the VTVL launcher

Stage	Parameter	Value
1st stage	Dry Mass	33.8 t
	Propellant Mass	378.0 t
	SI	8.95 %
2nd stage	Dry Mass	5.7 t
	Propellant Mass	60.2 t
	SI	9.5 %
Complete Launcher	**GLOM**	**479.0 t**

The total GLOM of the launcher is 479 tons, the total length is 67.25 m with a diameter of 4.8 m. In comparison, a Falcon 9 with a payload capability of 5.5 t into GTO has a GLOM of around 550 t. The first stage has a structural index (SI), which is here defined according to equation (1), of roughly 9%. Since no LOX/methane stages with similar propellant loading exist up to data, a comparison with other data is difficult. However, the SI is higher than that of the Falcon 9 (around 6%) with a first stage propellant loading of 411 tons using densified LOX and RP-1. Since the SI for LOX/methane is expected to be higher than that of LOX/RP-1 due to additional insulation and a more demanding propellant handling, the SI of the VTVL launcher seems to be in a reasonable range.

The mission profile of the VTVL launcher features the ascent phase of the 1st and 2nd stage until MECO. The reusable first stage then separates from the second stage which continues to accelerate to orbital velocity. Depending on the return mode (RTLS or downrange landing), the first stage then performs two to three major burns that alter its trajectory to meet the landing requirements. In the case of a downrange landing, only

two burns are necessary: one burn to reduce the re-entry loads once the stage hits denser parts of the atmosphere and one final landing burn to decelerate the stage to terminal landing velocity. In the case of an RTLS mission, a maneuver called “boostback” or “tossback” burn is performed after MECO. This maneuver reverses the horizontal velocity of the stage to ensure that it travels back towards the launch site. Fig. 6 shows the ascent and re-entry trajectories for barge and RTLS missions. The altitude vs. velocity profile of the VTVL stage is given in Fig. 10. Further limitations posed upon the descending stage are the following:

- Normal acceleration $n_z \leq 3$ g
- Convective maximum heat flux according to Fye-Ridell equation ≤ 140 kW/m² (with respect to a nose radius of 0.5 m)
- Maximum dynamic pressure ≤ 160 kPa
- Final landing velocity ≤ 2.5 m/s

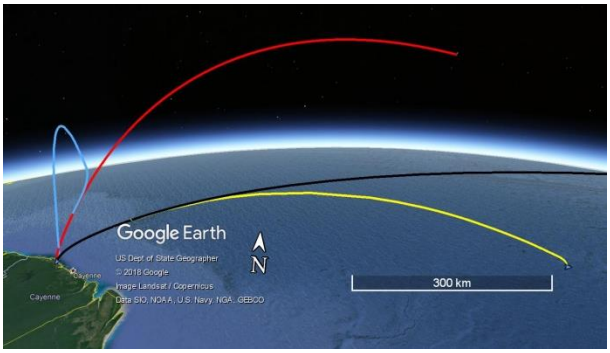

Fig. 6: Ascent and descent trajectories of a VTVL LEO mission with RTLS (ascent = red, descent = blue) and a GTO mission with barge landing (ascent = black, descent = yellow)

Since the VTVL concept requires the reignition of engines to perform the previously described re-entry and landing maneuvers, a certain amount of propellant is required for every RLV mission. The amount of propellant needed is mainly driven by the required energy to reach the specified target orbit. The higher the terminal energy, the more propellant has to be used for accelerating the payload; hence less propellant is available for descent. Furthermore, the payload performance is driven by the targeted landing strategy. In case of an RTLS maneuver, more propellant is required since the velocity vector has to be reversed. Contrary, a downrange landing demands less propellant. Fig. 7 shows the payload performance of the VTVL launcher into different target orbits as either expendable or reusable launch vehicle with downrange landing (DRL) or RTLS landing.

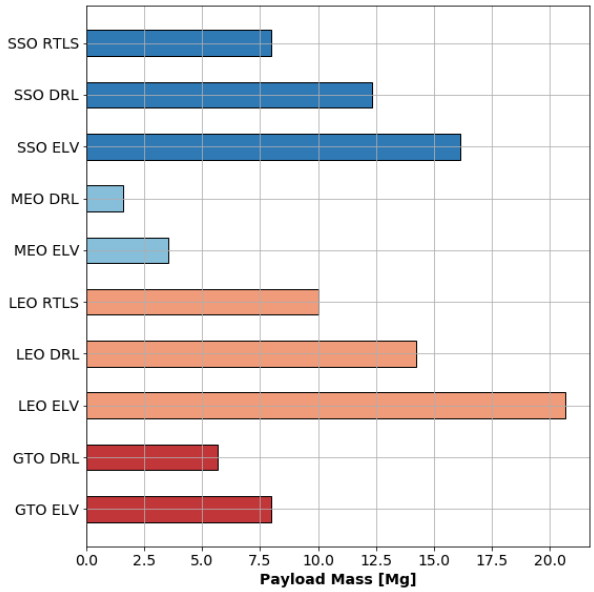

Fig. 7: Payload Performance of VTVL Launcher in different target orbits

A major advantage of the VTVL strategy is the high flexibility which is highlighted by the various different possibilities to service any specified orbit. The payload masses are 7.5 t to GTO as ELV, respectively 5.5 t to GTO as RLV, comparable to the Falcon 9 with a higher GLOM. LEO payloads range from 10 t to 20.5 t, thus serving roughly the same payload range as the Ariane 5. SSO payloads range from 7.5 t to 16 t, thus enabling either the launch of heavy SSO orbits or providing rideshare options for small to medium satellites. The payload into a MEO orbit typical for the Galileo satellites is between 1.7 t to 2.8 t, thus enabling the launcher to transport up to 4 Galileo satellites per launch.

Taking the market scenario from Table 1 into account the payload capabilities of the VTVL would lead to 10 launches of payload into GTO per year of which 3 launches would be as expendable launch vehicle (launches with 7 t payload mass). The Galileo missions to MEO could be covered by two reusable launches or one expendable launch, although in this case reusable would be preferred. SSO could be covered by one launch as RLV. Assuming that the final SSO differs or some restrictions occur 2 – 3 launches would be more reasonable. The LEO requirements can be served with two DRL launches, three RTLS launches or one DRL and one RTLS launch. Furthermore, one additional launch for BEO is foreseen although this launch should probably be as expendable launch vehicle. In summary, 15 – 18 launches would be necessary to serve the assumed market scenario. This is more than the current 8 – 10 Ariane 5 and Vega launchers per year combined. However, comparing the

launches required to the launch rate of a Falcon 9 (of around 20 per year as of 2018) and considering the fact that an RLV needs a higher launch rate to be economically viable, the baseline launch rate seems reasonable.

3.3. VTHL – System Design and Performance

Equal to the VTVL system, the VTHL system too is designed as TSTO configuration with a reusable winged first stage and an expendable stage in tandem configuration. The geometry and layout of the launcher is shown in Fig. 9. The first stage is propelled by 7 LOX/LH2 engines as described in Table 2. The engines are connected by a thrustframe to the LH2 tank of the first stage. The thrustframe is encapsulated by a skirt that serves only as aerodynamic shielding without transmitting any loads to the remaining structure. LOX and LH2 tank of the first and second stage are separated by a common bulkhead. In ascent configuration, with both stages attached to each other, the first stage's nose and second stage engine are covered by an interstage. After MECO the 1st stage is separated from the 2nd stage and begins its descent back to earth (see Fig. 8). The stage generates aerodynamic forces that decelerate the vehicle with a double-delta-wing structure. Furthermore, two vertical fins and a bodyflap are necessary to provide the required aerodynamic control during descent.

The VTHL launcher is planned to be recovered by "In-Air-Capturing" after re-entry (see Fig. 2). This method is based on the idea that a towing aircraft (e.g. modified Boeing 747) captures the returning RLV stage and tows it to the respective landing site, where the stage is released and performs an automatic and autonomous landing. Hence, a landing gear is required that shall be stored within the wing. The second stage design and layout is very similar to the second stage of the VTVL launcher from the previous section.

Fig. 8: VTHL reusable first stage in descent configuration

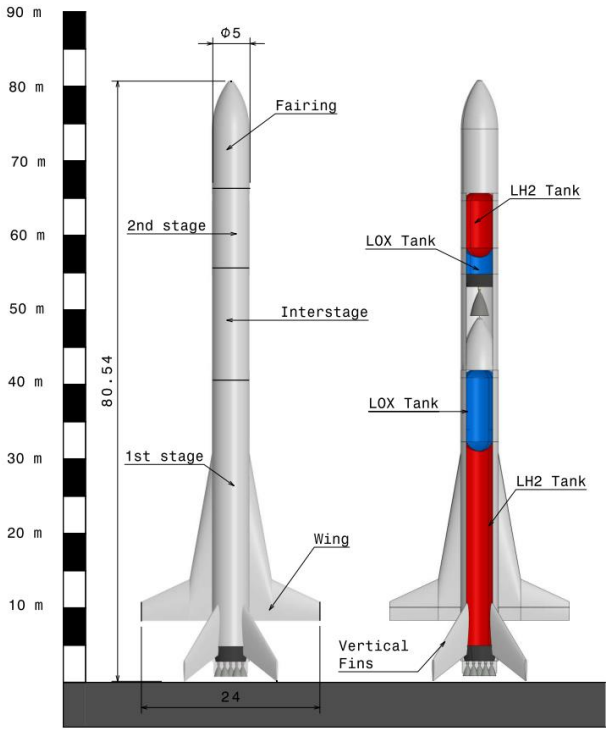

Fig. 9: VTHL launcher dimensions and internal layout

The mass breakdown of the VTHL launcher is presented in Table 4. Similar to the VTVL launcher, the masses of structural elements like tanks, interstage and skirts were subjected to a quasi-optimal optimization of stringer and frame geometry. The masses of wings, aerodynamic control surfaces and landing gear were estimated using empirical formulas from the in-house mass estimation tool *stsm*. The higher dry mass compared to the VTVL is due to the added wings, aerodynamic control surfaces and landing gear.

The dry mass is around 49.3 t with a propellant loading of 248.3 t. The SI is around 20% and thus around twice as high as the respective SI of the VTVL launcher. This is as expected and can be explained by the added dry mass by wings, aerodynamic control surfaces, TPS and landing gear. Furthermore, the use of LOX/LH2 leads to high SIs due to the low bulk density of the propellant combination. The second stage SI is 10.6% and thus at a value similar to the VTVL, although slightly higher due to a more powerful and heavy second stage engine.

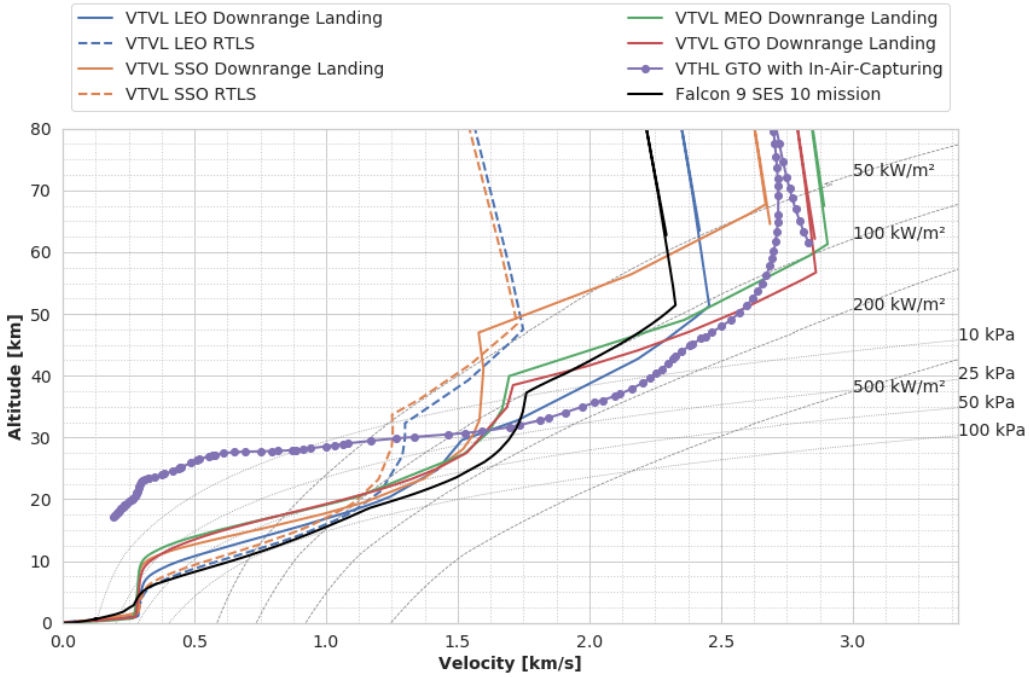

Fig. 10: Altitude vs. Velocity profile of the re-entry trajectories of the VTVL stage, the VTHL stage and the Falcon 9 SES 10 mission

Table 4: Mass breakdown of the VTHL launcher

Stage	Parameter	Value
1st stage	Dry Mass	49.3 t
	Propellant Mass	248.3 t
	SI	19.9 %
2nd stage	Dry Mass	6.4 t
	Propellant Mass [t]	60.3 t
	SI [-]	10.6 %
Complete Launcher	**GLOM [t]**	**377.8 t**

After MECO the RLV stage is separated from the second stage and coasts along a ballistic trajectory. Contrary to the VTVL stage the engines are not reignited and the deceleration of the stage is conducted via the aerodynamic forces produced by the vehicle (see Fig. 10 and Fig. 11). To produce sufficient aerodynamic forces a high initial AoA during re-entry is necessary. When approaching the point of maximum heat flux the AoA has to be gradually reduced to avoid skipping or bouncing off of the atmosphere. After transition to subsonic speed the AoA is reduced to a value where the lift-to-drag ratio L/D is at its maximum. This is optimal for the following In-Air-Capturing which should occur at minimum flight path angle corresponding to the maximum L/D ratio.

Due to the fact that the re-entry loads can't be controlled by reigniting the engines the maximum heat flux and dynamic pressure are driven strongly by the re-entry velocity and flight path angle. The TPS of the stage has to be designed to withstand said re-entry loads. Hence, no boundaries with respect to heat flux and dynamic pressure are set. However, a limitation of maximum 3 g of normal acceleration was set to not impose excessive stress on the structure.

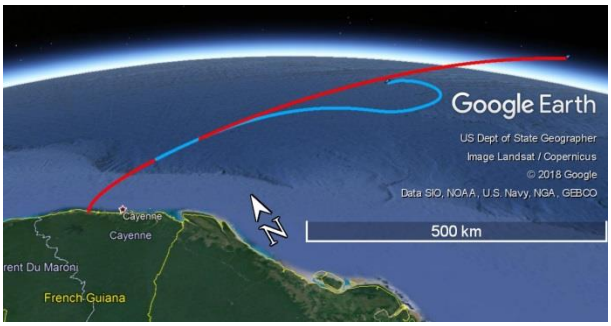

Fig. 11: Ascent and descent trajectories of a VTHL GTO (ascent = red, descent = blue)

The profiles of ascent and re-entry trajectories for a GTO mission are shown in Fig. 10 and Fig. 11. It is important to note that the re-entry trajectories of the VTHL stage were calculated for a GTO re-entry only so far. However, for different target orbits the conditions at MECO are almost identical (velocity, altitude, flight path angle) due to the fact that the initial transfer orbits are almost identical for all VTHL missions. It is clearly visible that the VTHL stage performs a heading change during re-entry which is initiated by banking the vehicle. This turn allows a reduction of downrange

distance from the stage to Kourou and thus facilitates the capturing and towback procedure.

The performances into the different orbits as described in section 0 are shown in Fig. 12. The VTHL is able to deliver more payload as RLV compared to the VTVL. The performances are in the heavy-lift segment and it is assumed that all nowadays typical payload masses and target orbits can be served. However, the diagram also highlights a difference from the VTHL to the VTVL, which is the reduced flexibility. Since the re-entry is controlled rather via aerodynamic forces without using the engines, the impact on payload performance is minimal but the possibility to differ from the nominal flight profile is limited.

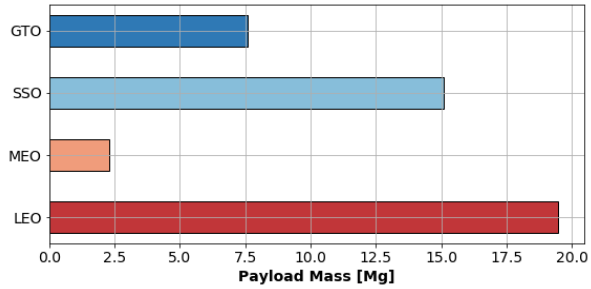

Fig. 12: Payload Performance of VTHL Launcher in different target orbits

As for the VTVL the payload capabilities with respect to the market scenario from Table 1 were considered. The payload capability of the launcher would lead to 9 – 10 GTO launches as RLV. 9 launches could be possible for dual launch configurations. The MEO payload could be delivered by 2 launches, the respective SSO payload in one launch or, assuming some restrictions or different final target orbits, 2 – 3 launches as for the VTVL. In the case of LEO missions, 2 launches would be necessary and one launch for the BEO mission respectively. In summary, the VTHL system would have a launch rate of 15-18 launches per year, thus being equal to the VTVL launch rate.

4. Aerodynamics and Aerothermodynamics

The geometries and trajectories described in the previous section were used to build and aerodynamic database (AEDB) and an aerothermodynamic database (AETDB). These databases are used to evaluate re-entry aerodynamics and loads and determine means to improve the RLV design.

4.1. VTVL

Aerodynamic Database (AEDB)

For the preparation of the extended database, the reference mission was analyzed and the main events, configuration and flight phases were defined. The computation matrix (Table 5) is based on the ascent and descent flight profiles corresponding to the reference mission trajectories (see Fig. 10).

Table 5: Computation Matrix for VTVL

Mach Number [-]	Ascent H_{ASC} [km]	Descent H_{DSC} [km]
0.6	3.1	0.5
0.8	4.7	0.8
1.2	8.1	11.3
1.5	10.4	13.1
2.0	13.8	15.0
3.0	21.6	18.1
4.0	29.8	21.4
5.0	38.1	27.0
7.0	52.3	44.1
10.0	75.1	85.1

VTVL and VTHL watertight models were created in order to build the aerodynamics domain for the following CFD computations. The ascent AEDB was calculated once without thrust and once with thrust (Fig. 13), implemented through a two-gas mixture (air & exhaust gas). The so called “ejector effect” of the jet plume increases the subsonic aerodynamic drag significantly (Fig. 14). In contrast, within the supersonic flight regime, the drag decreases.

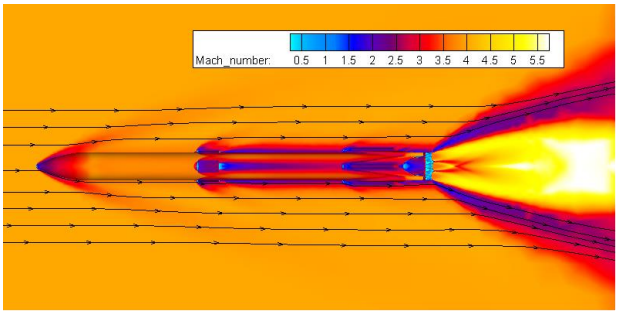

Fig. 13: VTVL with Thrust Plume

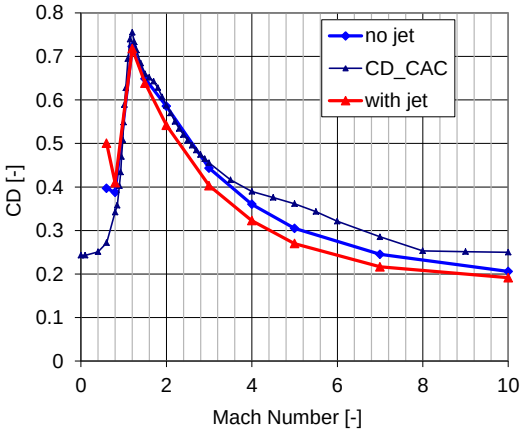

Fig. 14: Drag of the ascent configuration VTVL

Additionally, a controllability and stability analysis was performed for the VTVL descent configuration. Plain fins were chosen as trimming and control surface. Their size was determined to obtain the natural stability in the angle of attack range from 170° to 190° for the position of the in re-entry flight. During the launch phase the fins are folded.

An interesting observation is the fact that the thrust effect (engines on) during descent flight at AoA ≈ 180° dramatically (almost to 0!) reduces the aerodynamic drag (see Fig. 15). This effect must be taken into account for further mission simulations but are not yet included in the orbit calculations described in section 3. However, in the process of the ENTRAIN2 study these results shall be used to improve the VTVL design.

The generated AEDB allows flight path simulations for 3-DoF (point mass) as well as for the 6-DoF motion equations. The subsonic AEDB quality can be improved by the correction on the basis of the performed NS calculations described in the following section about the AETDB.

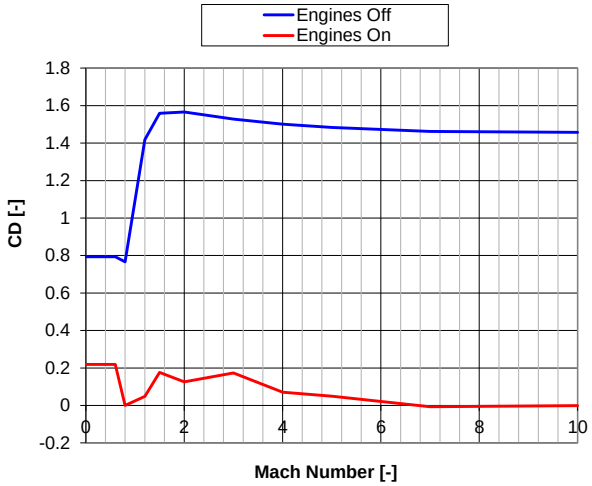

Fig. 15: Drag of the descent configuration VTVL

Aerothermodynamic Database (AETDB)

In the frame of the predesign based on engineering methods, ascent aerodynamics are modelled with empirical methods for simple fuselage wing combinations. Lift, drag and pitch moment coefficients as a function of angle of attack and Mach number in the subsonic, supersonic and hypersonic regimes are calculated. Methods for fuselage aerodynamics are based on slender body theory. Wing aerodynamics is based on empirical lifting line methods. Descent aerodynamics is analysed with empirical methods in subsonic and supersonic regimes and with a surface inclination tool in the hypersonic regime.

To improve the descent trajectory analysis, a comprehensive aerodynamic database for the entire Mach number range is generated using DLR´s TAU code. Aerodynamic coefficients are obtained by solving the inviscid Euler equations, utilizing a second order upwind flux discretization scheme together with a backward Euler relaxation solver.

For the VTVL launcher, 9 trajectory points were considered for the ascent phase and 11 for the re-entry and descent phase. The exhaust gas was treated as a reacting mixture of the combustion products of the Lox/Methane engine and the ambient air. Post-combustion, which occurs due to the fuel-rich operation of the propulsion system, was modelled based on a finite rate 3-step global reaction mechanism. A typical flow field result which corresponds to the initiation of the first retro-burn at an altitude of 56 km and a flight Mach number of 8.9 is shown in Fig. 16. The brown iso-surface indicates the extent of the exhaust gases which completely immerse the vehicle.

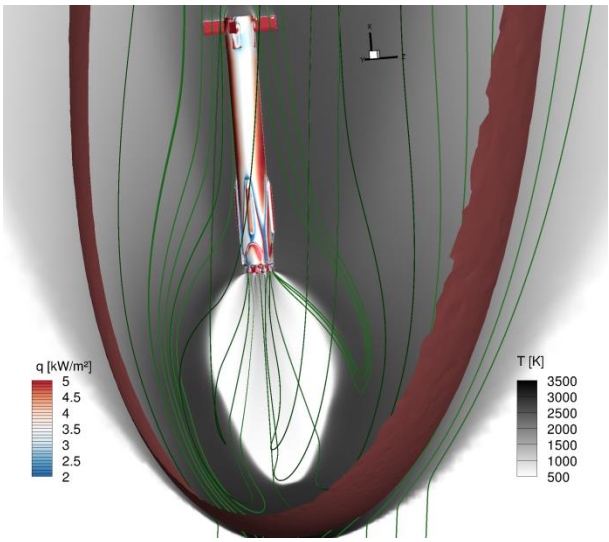

Fig. 16: Flow field and surface heat flux distribution for the VL-configuration immediately after initiation of first retro-propulsion manoeuvre

The heat loads during ascent are generally lower as during descent. Significant base heating occurs only during high-altitude flight where the associated large spreading of the exhaust plumes results in a strong recirculation of hot exhaust gases towards the rocket structure.

During descent, global peak heating occurs during the un-propelled high-speed flight. While the exhaust plume during retro-burns efficiently shields the base region of the rocket from excessive thermal loads, it generates high heat fluxes at the protrusions and control surface leading edges. The maximum surface temperatures which are reached during re-entry at a flight time of approximately 300 seconds are shown in Fig. 17. A simple lumped-mass model (5 mm Aluminium structure) was employed to generate this data. Major heating occurs only at the base plate, the upstream protrusions of the landing leg structure and the

leading edges of the control surfaces. The complex flow patterns during re-entry result in strong gradients of surface heat fluxes and surface temperatures. Especially during the un-propelled flight, strong vortex systems are formed as the flow passes through the cluster of thrust nozzles. The footprints of these vortex systems generate complex heating patterns which result in the occurrence of hot spots primarily at the upstream surface of the landing legs (see Fig. 17).

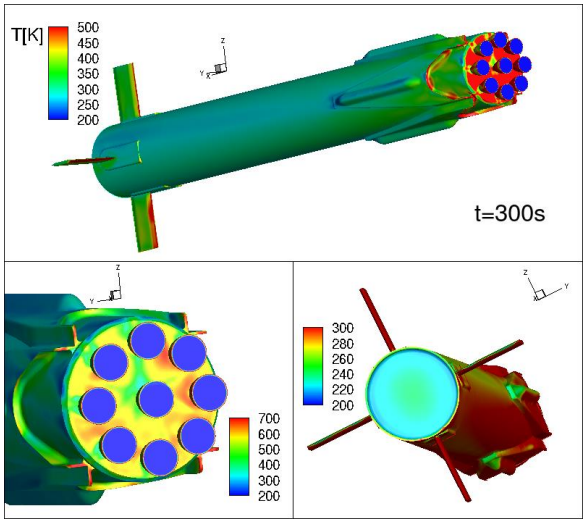

Fig. 17: Maximum surface temperatures of the VL-configuration resulting from the lumped mass model

4.2. VTHL

Aerodynamic Database (AEDB)

Similar to the VTVL-configuration the computation matrix for the VTHL (Table 6) is based on the re-entry flight profile of the VTHL launcher (see Fig. 10). Providing stability, controllability and trimability of the reusable winged stage with sufficient L/D is the main objective of the aerodynamic design for the VTHL configuration.

Table 6: Computation Matrix for VTHL

Mach Number [-]	Descent H_{DSC} [km]
0.5	5.0
0.7	17.3
0.9	19.8
1.2	23.7
1.5	25.0
2.0	27.5
3.0	28.0
4.0	29.6
6.0	33.0
9.0	70.0

According to the computation matrix, calculations were performed with three different geometries having negative, neutral and positive flap deflection angles. The maximum allowed absolute flap deflection magnitude is 20°. The body flap does have positive deflection angles only (downward deflection). To obtain aerodynamic coefficients at trimmed conditions, interim values of the aerodynamic coefficients are linearly interpolated within the mentioned extrema and zero positions. Thus, the flap trim-deflection δ_{trim} was found as solution of the non-linear moment equation: Cm (Ma, α, δ_{trim}) = 0.

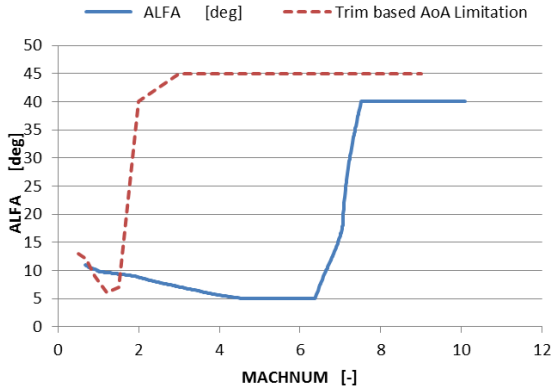

Fig. 18: Descent trajectory for VTHL with trim boundaries

The deflections limitations -20° < δ_{trim} < +20° estimate the range of trimability (see Fig. 18). The descent configuration is trimable for AOA values from -5° to +45° within the Mach range 2 to 9. However, natural stability is only provided for Mach numbers Ma = 0.5 by AOA < 12°, for Ma = 0.9 by AOA < 9° and for 1.2 < Ma < 15. by AOA < 6°. Hence, the current re-entry trajectory would either have to be adapted to fly at trimable AoAs or the RLV stage design would have to be changed. Either the wing position and design could be altered or a GNC system that would be able to handle unstable flight conditions could be possible solutions.

As shown in Fig. 19 and

Fig. 20, L/D is significantly reduced through the trimming losses by the flap deflections. In the subsonic case the available L/D reduces by nearly 50% (from 6 down to 3.4).

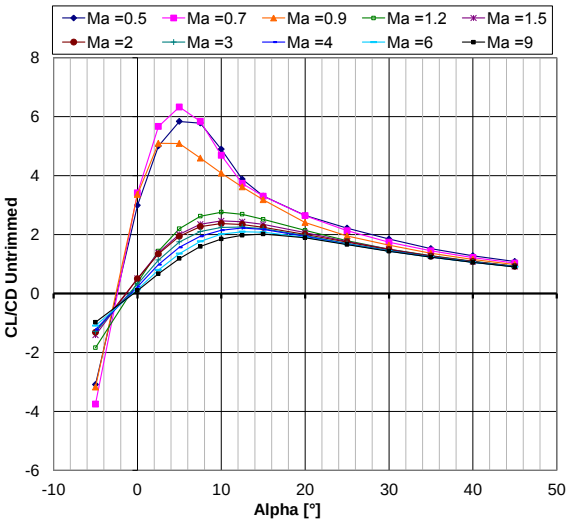

Fig. 19: CL/CD– w/o Trim Deflection

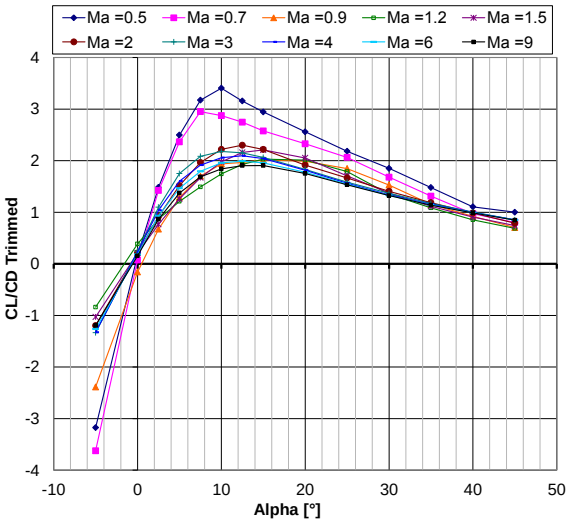

Fig. 20: CL/CD– with Trim Deflection

Aerothermodynamic Database

A similar approach for the generation of the AETDB was applied to the HL-configuration. As a result of mesh sensitivity analysis an unstructured mesh with 820*10³ nodes was chosen as a trade-off between solution accuracy and calculation time. The calculation points are extracted from a reference trajectory with Mach number ranging from 0.5 to 9. The angle of attack values range from -10° up to +45°. The pressure coefficient distribution for a subsonic flight point is shown in Fig. 21. The pressure distribution shown is for a subsonic cruise flight point in 5 km altitude at a Mach number of 0.5. The respective angle of attack is 5°. The area of low pressure coefficients at the outer wing leading edge is clearly visible. This constitutes a potential problem concerning the choice of airfoil section for the outer wing segment. In the frame of the configuration predesign the RAE2822 airfoil has been selected, as described in section 3. Due to the airfoil geometry – in particular the small airfoil nose radius – and the rather high angle of attack for subsonic cruise flight the flow acceleration on the upper airfoil surface in the vicinity of the leading edge is very strong. This has the potential to make the flow partially supersonic which is also shown by RANS calculations. Thus the choice of airfoil section will be reassessed during subsequent design iterations.

Similar to the EULER calculations for the AEDB the AETDB was calculated for different flap deflections up to a maximum magnitude of deflection of 20°. The descent aerodynamic database consists of 140 calculations for each flaps setting. The validation of the Euler results is done by RANS calculations for specific flight points. For the ascent configuration the influence of running rocket engines and their exhaust gas jets on aerodynamic drag is analysed by a two gas simulation. For the rocket engine exhaust gas properties average values corresponding to the respective combustion products are used. The ascent calculations feature no flap deflection. For the reference ascent trajectory 90 calculations are performed.

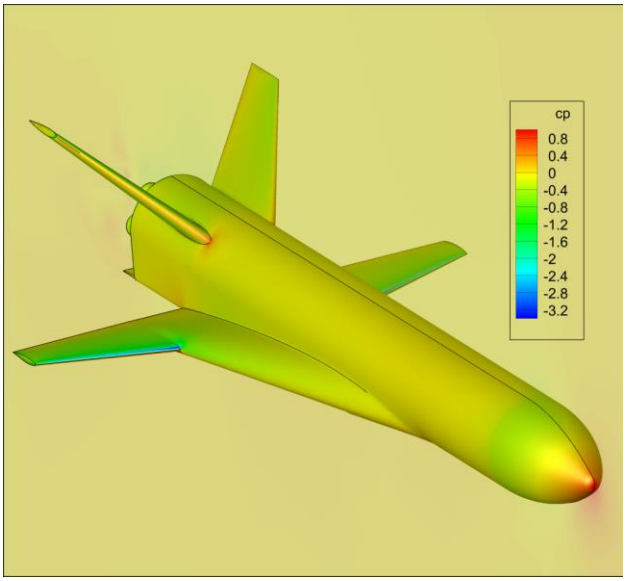

Fig. 21: Pressure coefficient distribution H245 stage (Mach=0.5, Altitude=5 km, AoA=5.0°)

The assessment of heat loads during atmospheric re-entry is necessary to allow for the detailed thermal protection system design. For the HL-configuration, this heat loads database was created based on eleven trajectory points of the reference descent trajectory. The heating predictions are based on viscous CFD simulations with fully resolved boundary layers. Turbulence is modelled using a one-equation RANS approach. Thermodynamics is treated with an

equilibrium gas model which includes high temperature effects such as vibrational excitation of the molecules and chemical dissociation. Four initial wall temperatures from 200 K to 1100 K are considered. An exemplary heat flux distribution for the peak heating flight point is shown in Fig. 22. The resulting heat fluxes amount to approximately 200 kW/m² and 400 kW/m² in the nose area and at the wing leading edges, respectively.

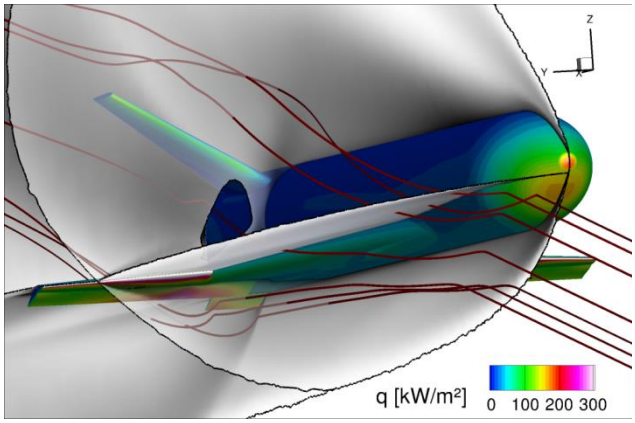

Fig. 22: Heat flux distribution for the peak heating flight point (Mach = 6.8, Altitude = 37.6 km, AoA=12°)

The entirety of the obtained heat flux data is organized in a data base which, together with appropriate interpolation algorithms, forms a complete surrogate model for the aerothermal heating of the vehicle. The local heat flux distribution can be obtained for any flight time and any surface temperature distribution. This surrogate model can be easily coupled to transient structural analysis tools to calculate local surface temperature evolutions during the re-entry flight. Results in form of a temperature distribution are shown in Fig. 23. The structural heating response was treated with a simple lumped-mass model (corresponding to an aluminium structure with a thickness of 5 mm). The initial surface temperature at t=0s was assumed to be 200 K. The results in Fig. 23 show the maximum surface temperatures which occur at an altitude of around 30 km and a Mach number of approximately 4.4. It should be noted that this flight point is different from the point of maximum nose stagnation point heat flux at an altitude of 37.6 km. Critical components of the vehicle are the control surfaces, the leading edges of the outer wings and rudders as well as the vehicle nose.

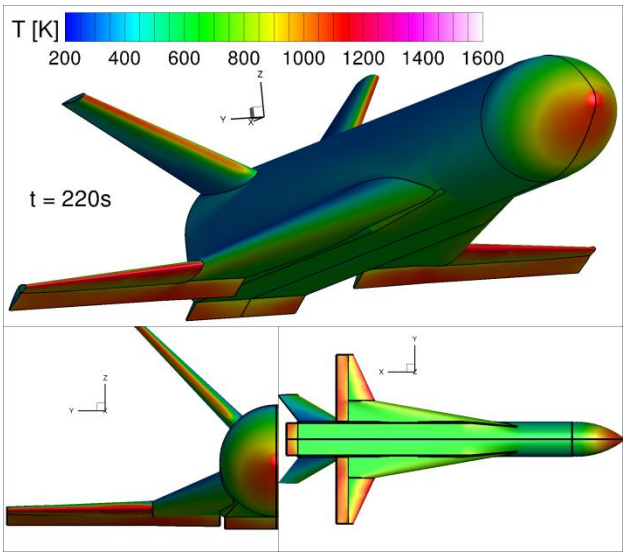

Fig. 23: Temperature distribution resulting from a simple lumped-mass model (occurring at a flight time of 220 s)

5. System Dynamics, Guidance, and Control

For the systematic assessment of the chosen reference configurations in terms of system dynamics, guidance, and control, multi-disciplinary and multi-fidelity studies have to be performed. For this purpose, modular but consistent multibody models for both concepts have been implemented using dedicated frameworks and tools as described in [11]-[13] and [16].

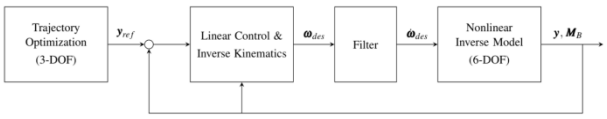

Fig. 24: Intermediate 6-DOF Modeling Approach using Nonlinear Inverse Models [13].

For the VTVL configuration, the multi-disciplinary and multi-fidelity modeling approach as depicted in Fig. 24 is used to evaluate the launch vehicle's performance. First, 3-DOF models are generated using the object-oriented modeling language *Modelica* [9]. These launch vehicle models are translated into so-called *Functional Mock-up Units* [10], which can be integrated into the Matlab-based multi-objective and multi-phase trajectory optimization package *MOPS trajOpt* as introduced in [14] and [15]. In this context, the launch vehicle models can be upgraded and extended individually in order to address dedicated analysis requirements; for instance for the computation of orbital parameters to study their influence on the optimized trajectory and vehicle performance.

Furthermore, the resulting reference trajectory provides optimal guidance commands (e.g. aerodynamic angles), which are used to compute the desired angular velocities with a feedback control loop and kinematic inversion automatically performed by *Modelica*. These inputs are then applied to multi-fidelity nonlinear inverse models, which can guarantee consistency with the 3-DOF model used within the trajectory optimization. If required, the nonlinear inverse model can be replaced by a range of 1-DOF to 6-DOF models by exchanging the underlying kinematics formulation. Finally, the required moments to perform a desired maneuver are obtained from the nonlinear inverse model.

In addition to the requirements presented in the previous sections, the following aspects were considered:

- The payload mass shall be maximized.
- The fuel used for the return flight shall be minimized while allowing the exchange with fuel used for the main stage during ascent.
- In the upper stage, the propellant mass may be traded for the payload mass.
- A circular geostationary transfer orbit has to be reached with an apogee and perigee of 250 km × 250 km, and an inclination of 6°.
- The downrange landing has to be guaranteed within an altitude of approximately 35 m to 60 m and a final velocity below 8 m/s.
- The heat flux at fairing separation shall be lower than 1540 W/m².
- The remaining descent propellant at the end has to be at least 900 kg for the final landing maneuver.

The final results of the trajectory optimization for the combined ascent and descent of the VTVL concept are discussed in [16], while only a subset of results is shown in Fig. 25. The dashed red line represents the ascent of the full vehicle, while the dotted green line shows the ascent of the upper stage into the target orbit and the blue line depicts the descent and vertical landing of the first stage. The flight path angle highlights the vertical take-off (90°) and vertical landing (-90°). Additionally, the influence of the argument of perigee on the overall optimized flight trajectory, as well as a return approach by only using one engine instead of three engines for the final landing maneuver have been evaluated within the ENTRAIN study.

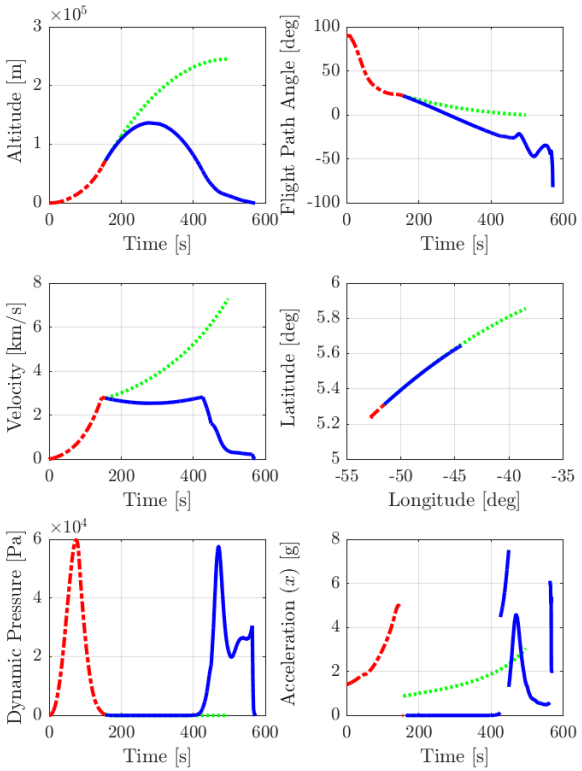

Fig. 25: Optimized Trajectory of the Combined Ascent and Descent Flight of the VTVL Configuration [16].

For preliminary design studies, an accurate estimation of the overall moment budgeting is required. Since a full aerodynamic coefficient matrix is often not available during preliminary design studies, the fidelity level of the flight dynamics models has to be adapted to the availability of the aerodynamic coefficients. For this purpose, multi-fidelity models were used for moment estimation and angular impulse computation of the flip-over maneuver. In this case, the flight trajectory as obtained by *TOSCA* (compare Fig. 10) was chosen, while considering a simplified assumption of the moment of inertia and by using the aerodynamic axial, normal and pitch moment coefficients. The influence of the aerodynamic control surfaces is not taken into account, such that the required moments have to be generated by the RCS only.

As discussed in [16], the 1-DOF model uses only the pitch angle and pitch rate as states, while the 4-DOF model additionally considers all translational states. The remaining degrees of freedom are then provided by the reference trajectory and assigned ideally to the flight dynamics model. In contrast to the 1-DOF and 4-DOF models, the 6-DOF model considers all translational and rotational states. The results in Fig. 26 showcase that all models follow the reference trajectory with small

deviations which is demonstrated by the normalized angular impulse.

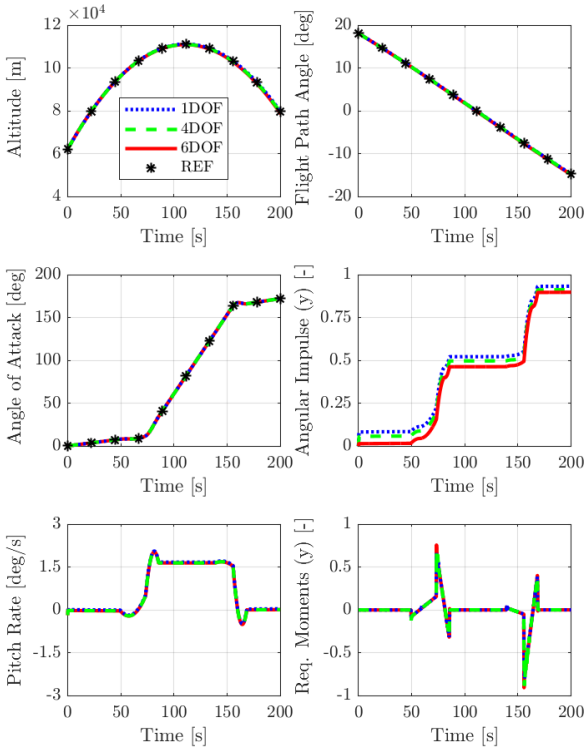

Fig. 26: Computation of Required Moments to perform the Flip-Over Maneuver during Descent.

Currently, trajectory optimization and controllability studies of the VTHL configuration are performed using a similar approach as discussed in [11]-[13] and [16]. For this purpose, methods are developed which enable the computation of aerodynamic deflection angles from multi-dimensional aerodynamic datasets based on the required moments as presented above.

6. Conclusion

In this paper, potential future reusable launchers have been investigated in detail to determine technical challenges and their impact on an RLV design. Hence, two different promising concepts of reusing first stages, namely VTVL and VTHL, were applied to a launcher design according to preliminary design and mission assumptions. The goal is to enhance the know-how about RLV launcher design and the necessary technologies and to get closer to designing a feasible European launcher.

In this context, designs based on the results from the first phase of the ENTRAIN study were used and two different launchers were derived: a launcher with a reusable vertical landing first stage (VTVL) and another one with a horizontal landing first stage (VTHL). The VTVL stage is propelled by LOX/LCH4 in the first stage and LOX/LH2 in the second stage. The VTHL launcher is propelled by LOX/LH2 in both stages and the first stage returns by In-Air-Capturing.

Those two investigated launchers were designed with a target payload mass of 7.5 tons to GTO. The VTHL launcher is able to deliver this payload as RLV, the respective VTVL launcher was designed to deliver 5.5 t as RLV and 7.5 t to GTO as ELV. This allows a high flexibility according to the required mission but also negates some of the advantages of an RLV (cost reduction) by expending the stage. The VTHL launcher has a GLOM of around 378 t, the VTVL a GLOM of 479 t. The low GLOM of the VTHL launcher is explained by the use of LOX/LH2 as propellant in both stages, thus taking advantage of the high Isp. Another driver of the higher mass for the VTVL system arises from the fact that the propellant necessary for the re-entry burns and manoeuvres has to be accelerated during the ascent phase, whereas the VTHL launcher uses all its fuel for accelerating the launcher. Both launchers are able to cover a payload range that allows them to service a market scenario with a reasonable number of launchers per year in comparison to current Ariane 5 and Falcon 9 operations.

Following the preliminary design and performance estimation, both RLV concepts were investigated considering the aerodynamic and aerothermodynamic behaviour during re-entry. This aspect of any RLV design is considered the most critical since the resulting TPS and re-entry loads have a major impact on the refurbishment effort and costs. The investigation of re-entry loads was conducted using CFD analysis. An interesting observation of said analysis was that the drag of the VTVL stage is close to zero during any burn maneuvers. Furthermore, several regions of critical temperatures were identified. Those are the baseplate covering the engines, the landing legs protrusions such as the grid fin leading edges. These regions have to be structurally reinforced to be able to deal with the re-entry loads without requiring extensive refurbishment between flights.

For the VTHL, several phenomena that have an impact on launcher design could also be identified. First, a potential shock-shock interaction between the fuselage shock and the wing's leading edge shock leads to locally elevated heatflux values. The region of potential impact has to be covered with a stronger TPS compared to the unaffected areas of the wing or possible morphing wing structures could be imagined [17]. Further critical parts during re-entry are the nose, the rudder's leading edges and the control surfaces. Furthermore, the wing position will have to be re-evaluated since unstable trim points were identified within the current re-entry trajectory.

While the results shown above indicate that the current designs are indeed feasible the need for

refinement and optimization is large. For example: Both VTHL and VTVL control the encountered heatflux with aerodynamic (VTHL) or propulsive (VTVL) deceleration. With additional wing surfaces or a longer re-entry burn the heat fluxes could be kept very low. While this would add inert mass to the system it would also decrease the mass of the thermal protection systems. In order to find the solution the AETDB would have to be generated for multiple reference trajectories and aerodynamic shapes, an effort not feasible in this type of early system study. The curse of dimensionality would make this a substantial task even for a full development program. This is only one example of the many possibilities for optimization. Nevertheless, the scope of the ENTRAIN2 study allows for a more detailed investigation of RLV challenges. In this first loop, some of those challenges were identified and are to be used to refine the RLVs' design in the further course of the study.

However, a major uncertainty remains when evaluating and comparing these types of vehicles: A reliable assessment of cost. The principal goal of any RLV development is the reduction of cost. In order to achieve this goal the launcher has to be designed in a cost optimal manner. Given the very large uncertainties in cost estimation, especially for RLV, this is currently unfeasible. However, preliminary assessment of costs has been already started at DLR [18]. Individual components can, of course, be optimized for cost, but this is not possible for the entire system. There is a large need for reliable and accurate cost estimations methodologies in order to evaluate different design options beyond the technical level.

References

[1] J. Wilken, S. Stappert, L. Bussler, M. Sippel, E. Dumont, "Future European Reusable Booster Stages: Evaluation of VTHL and VTVL Return Methods", 69th IAC, Bremen , Germany, 2018

[2] S. Stappert, J. Wilken, L. Bussler, M. Sippel, A Systematic Comparison of Reusable First Stage Return Options, 8th European Conference for Aeronautics and Space, Madrid, Spain, July 2019

[3] Sippel, M.; Stappert, S.; Bussler, L; Krause, S.; Cain, S.; Espuch, J.; Buckingham, S.; Penev, V.: Highly Efficient RLV-Return Mode "In-Air-Capturing" Progressing by Preparation of Subscale Flight Tests, 8th EUROPEAN CONFERENCE FOR AERONAUTICS AND SPACE SCIENCES (EUCASS) , Madrid July 2019

[4] L. Bussler, S. Stappert, J. Wilken, M. Sippel, I. Dietlein: Analysis of VTVL and VTHL Reusable Launch Vehicle Configurations, International Conference on Flight vehicles, Aerothermodynamics and Re-entry Missions and Engineering (FAR), Monopoli, Italy, 2019

[5] J. Wilken, S. Stappert, "Investigation of a European Reusable VTVL First Stage", 8th European Conference for Aeronautics and Space, Madrid, Spain, July 2019

[6] Stappert, S., Wilken, J., Sippel, M., Dumont, E., "Assessment of European Reusable VTVL Booster Stage", Space Propulsion Conference, Seville, Spain, 2018

[7] E. Dumont et al., "CALLISTO – Reusable VTVL launcher first stage demonstrator", Space Propulsion Conference, Seville, Spain, 2018

[8] S. Stappert, M. Sippel, "Critical Analysis of SpaceX Falcon 9 v1.2 Launcher and Missions", DLR SART TN-009/2017, DLR, 2017

[9] Modelica Association, "Modelica – A Unified Object-oriented Language for Physical Systems Modeling," Language Specification 3.4, 2017.

[10] Modelica Association, "Functional Mock-Up Interface for Model Exchange and Co-Simulation," 2015.

[11] L. E. Briese, K. Schnepper, and P. Acquatella B., "Advanced Modeling and Trajectory Optimization Framework for Reusable Launch Vehicles," in IEEE Aerospace Conference, 2018.

[12] P. Acquatella B., L. E. Briese, and K. Schnepper, "Guidance Command Generation and Nonlinear Dynamic Inversion Control for Reusable Launch Vehicles," 69th International Astronautical Congress, 2018

[13] L. E. Briese, P. Acquatella B., and K. Schnepper, "Multidisciplinary Modeling and Simulation Framework for Reusable Launch Vehicle System Dynamics and Control," in 7th International Conference on Astrodynamics Tools and Techniques (ICATT), 2018.

[14] K. Schnepper, "Trajektorienoptimierung in MOPS – Das Paket trajOpt Version 1.0," Tech. Rep., DLR German Aerospace Center, 2014.

[15] H.-D. Joos, "MOPS – Multi-Objective Parameter Synthesis," Tech. Rep. DLR-IB-SR-OP-2016-128, DLR German Aerospace Center, 2016.

[16] L. E. Briese, K. Schnepper, "Multi-Disciplinary and Multi-Fidelity Evaluation of VTVL and VTHL Reusable Launch Vehicle Configurations," International Conference on Flight Vehicles, Aerothermodynamics and Re-entry Missions & Engineering (FAR), 2019.

[17] M. Sippel, S. Stappert, L. Bussler, C. Messe: Powerful & Flexible Future Launchers in 2- or 3-stage Configuration, IAC-19-D2.4.8, Washington DC, October 2019

[18] S. Stappert, J. Wilken, L. Bussler, M. Sippel, A Systematic Assessment and Comparison of

Reusable First Stage Return Options, 70th International Astronautical Congress, Washington DC, USA, 21st – 26th October 2019